Emission Control Science and Technology (2019) 5:307–316
https://doi.org/10.1007/s40825-019-00141-2

SPECIAL ISSUE: IN RECOGNITION OF PROFESSOR WOLFGANG GRÜNERT'S CONTRIBUTIONS TO THE SCIENCE AND FUNDAMENTALS OF SELECTIVE CATALYTIC REDUCTION OF NOX

# Design of a Reactor Cell for Modulated Excitation Raman and Diffuse Reflectance Studies of Selective Catalytic Reduction Catalysts

Rob Jeremiah G. Nuguid [1,2] · Davide Ferri [1] · Oliver Kröcher [1,2]

Received: 23 May 2019 / Revised: 30 August 2019 / Accepted: 6 September 2019 / Published online: 14 October 2019
© Springer Nature Switzerland AG 2019

**Abstract**
Despite the large pool of spectroscopic studies about selective catalytic reduction (SCR), transient response experiments have not yet been fully utilized to extract key mechanistic and kinetic insights. Here, we describe the construction and performance characteristics of a spectroscopic cell that can be used for such an experimental design. The rapid gas exchange in the reaction chamber of the cell makes it amenable to modulated excitation (ME) experimentation. We show case studies wherein this cell was used for Raman, visible, and infrared spectroscopy under ME conditions to investigate the SCR mechanism over three of the most industrially relevant SCR catalysts today—$V_2O_5/TiO_2$, Cu-SSZ-13, and Fe-ZSM-5.

**Keywords** Infrared spectroscopy · Mechanism · Modulated excitation · Operando spectroscopy · Raman spectroscopy · Selective catalytic reduction · UV–visible spectroscopy

## 1 Introduction

Nitrogen oxide ($NO_x$) abatement has always occupied a central position in emission control research [1–4]. The active interest in this topic originates from the detrimental effects of $NO_x$ to human health and the environment. Unmitigated $NO_x$ pollution not only causes respiratory diseases but also contributes to ozone layer depletion, photochemical smog formation, and acid rain. Over the years, several $NO_x$ abatement strategies have been proposed, and some of them have been successfully commercialized [5–7]. Selective catalytic reduction (SCR) is currently the most efficient one [8], and the only viable option for diesel-powered vehicles and thermal power plants. In this process, the selective reductant $NH_3$ is used to transform $NO_x$ into environmentally benign molecules. Approximately 90% of the $NO_x$ emissions are in the form of NO [9] and correspondingly, the primary reaction that occurs on the catalytic converter is as follows:

$$4\,NO + 4\,NH_3 + O_2 \rightarrow 4\,N_2 + 6\,H_2O \quad (1)$$

The presence of $NO_2$ in the feed can also give rise to the *fast* SCR reaction:

$$2\,NO + 2\,NO_2 + 4\,NH_3 \rightarrow 4\,N_2 + 6\,H_2O \quad (2)$$

which occurs at least one order of magnitude faster than Eq. 1 [10]. Diesel oxidation catalysts are positioned in vehicles upstream of an SCR system to partially oxidize NO into $NO_2$, and allow the *fast* SCR reaction to proceed.

Various types of SCR catalysts are commercially available. Since the 1970s, $V_2O_5/TiO_2$-based materials have remained to be the most widely used for stationary applications. Their industrial success stems from their high activity, good resistance to $SO_2$ poisoning, and moderate cost [11]. However, metal-exchanged zeolites have emerged as the preferred

**Electronic supplementary material** The online version of this article (https://doi.org/10.1007/s40825-019-00141-2) contains supplementary material, which is available to authorized users.

✉ Davide Ferri
davide.ferri@psi.ch

[1] Paul Scherrer Institut, CH-5232 Villigen PSI, Switzerland

[2] Institute of Chemical Sciences and Engineering, École polytechnique fédérale de Lausanne (EPFL), CH-1015 Lausanne, Switzerland

option in automotive systems because they are more adaptable to high space velocity conditions [8]. Cu-based catalysts in particular possess superior activity in the low temperature regime, which is essential for cold start-up and short-distance driving. ZSM-5 was initially used as the zeolite support, but it had poor stability in the presence of $H_2O$ or hydrocarbons [12]. Nowadays, the preference for SSZ-13 as the carrier for Cu is justified by the relatively smaller pores of the zeolite, thereby ensuring unparalleled hydrothermal stability [13, 14]. Fe-exchanged zeolites have also received attention because of their high activity at higher temperatures: above 450 °C, Fe-ZSM-5 outperforms its Cu counterpart in terms of NO conversion [15]. Fe catalysts are also considerably less susceptible to $N_2O$ formation than Cu catalysts, especially at low $NO_2$ feed concentration [16].

The scientific literature abounds with spectroscopic investigations of SCR catalysts, and several debated reaction mechanisms have been proposed based on these studies [17–19]. However, most of these experiments were carried out under steady-state conditions, which are not sufficient to extract in-depth mechanistic and kinetic details about the system beyond the ones achieved so far. Furthermore, real-life automotive catalysts operate under dynamic conditions of temperature, pressure, and reactant composition that are dictated by the driving conditions. Mobile urea-SCR installations for instance rely on periodic urea injection to generate $NH_3$. Lastly, isolation of the structure of the catalytically active species within the large contribution of stationary species remains a challenge.

The aforementioned difficulties can be addressed in laboratory studies by the use of transient spectroscopic methods and, in some cases, modulated excitation (ME) conditions wherein the concentration of one of the reactants is varied repeatedly as a function of time [20]. These experiments rely on the sudden variation of the experimental conditions to induce the largest spectroscopic response in the system. Beside spectrometers with a high temporal resolution and the use of switching valves with sub-second response time, a suitable reactor cell with a low void volume is needed—a requirement that most commercial spectroscopic cells lack. Although commercial cells are suitable for routine in situ studies, they cannot exchange gases fast enough for transient response experiments. Special sample holders must be custom-built for this purpose, and various examples exist [21–27].

In mechanistic studies, no single spectroscopic or diffraction technique is self-sufficient. A comprehensive molecular view of the SCR reaction can only be developed from the complementary information offered by different techniques. Raman spectroscopy can directly probe the molecular structure of the catalyst, especially in metal oxide-based systems. Due to their highly polarizable bonds, transition metal oxides typically give rise to Raman-active modes with intense signals [28]. Ultraviolet–visible (UV–Vis) spectroscopy delivers electronic information about the metal active sites. It is especially useful to monitor changes in the oxidation state as many transition metals have characteristic weak *d-d* transition and intense charge transfer bands in the visible and UV region of the spectrum, respectively [29]. Infrared spectroscopy is the technique of choice to follow the evolution of adsorbed chemical species on a catalyst surface—from the formation of intermediates to the release of products [28, 30].

Here, we describe in detail the design and characteristics of a custom-built spectroscopic cell with a reduced void volume. Coupled to a suitable set-up, this cell can be used to repeat the same type of experiment using complementary spectroscopic methods. We demonstrate that the fabricated cell accomplishes its intended purpose for carrying out transient response and ME studies.

## 2 Methods and Materials

### 2.1 Cell Design and Experimental Set-up

The cell is presented in Fig. 1 and was constructed according to the specifications given in Figs. S-1 to S-4. An actual image of the cell is presented in Fig. S-5. It is based on the design of a Harrick Scientific spectroscopic cell and is used with a Praying Mantis™ accessory for diffuse reflection. The cell can be easily adapted to be used with automatic stages for mapping experiments similar to the commercial cell. Two major innovations contribute to reduce the void volume significantly in the cell. First, the cell body (A; Fig. 1) was redesigned to remove the inner void volume present in the commercial cell. This was achieved by positioning the heat cartridge vertically and exploiting it to pre-heat the gas feed to the sample. The body confining the heating cartridge (B) also contains the sample cup (C). The gas feed runs within an annular void space of approximately 4 mL between A and B before meeting the sample in a very similar geometry to the commercial cell. In the current design, the thermocouple used to control the sample temperature (D) is inserted approximately 1 mm below the sample cup in the same body, while a second thermocouple (E) is placed parallel to this one and is used to record the temperature. For improved temperature control and monitoring, another thermocouple may be inserted perpendicular to the sample cup. Second, the cell cover consists of just one flat window (F) instead of two windows arranged in a dome-like configuration, as it is the case in the commercial cell. Although this geometry is not optimum for diffuse reflectance because of the specular component, the cell can be lifted up until the signals of the sample—and not necessarily the amplitude of the IR signal—are maximized. This is shown in Fig. 2 for a zeolite sample. The IR signals from the zeolite framework are clearly discernible in the single beam spectrum from 2000 to 1000 $cm^{-1}$. We have also

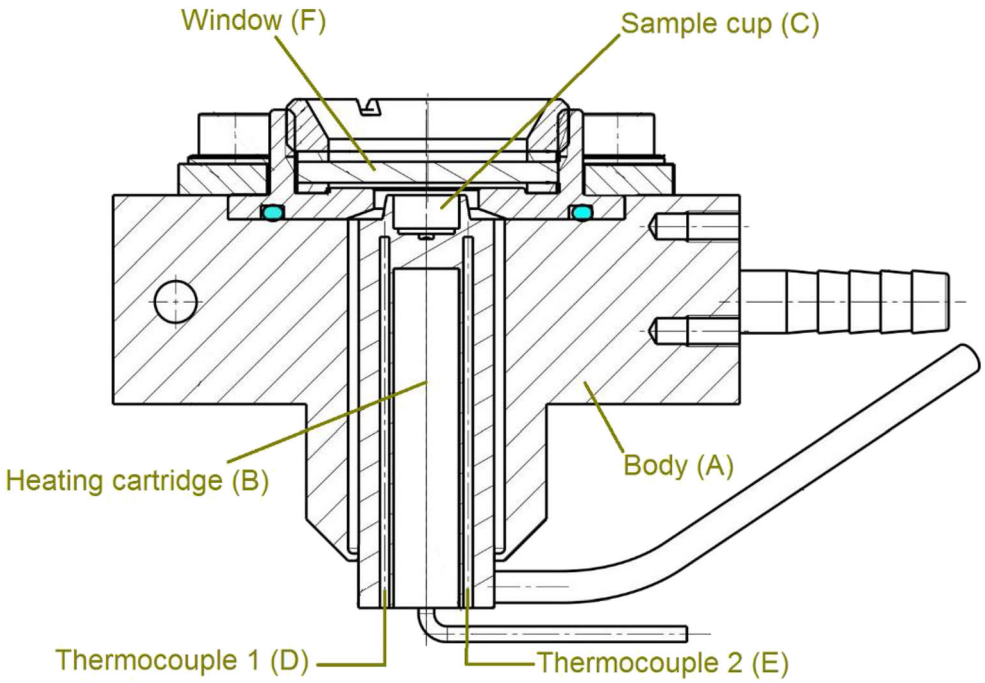


**Fig. 1** Design of the spectroscopic cell. All the detailed specifications and measurements are given in Figs. S-1 to S-4

exploited this geometry successfully in a different cell design [24]. The moveable clamps used to secure the window on top of the spectroscopic cell follow the design of the commercial cell.

We have demonstrated earlier that the cell can be used as a reactor for SCR studies [31–33]. The cell is the heart of the setup consisting of a main gas feed line and four auxiliary lines. The gas through the auxiliary lines can be mixed with the one flowing through the main line using four independent solenoid valves (5 ms response, Series 9; Parker) controlled by the Rapid Scan TRS mode of the OPUS spectroscopy software (Bruker). The exit of the cell can be interfaced with an IR spectrometer or a mass spectrometer. All lines are stainless steel. Water is generated in situ from precise flows of $H_2$ and $O_2$ through a $Pt/Al_2O_3$ catalyst. This allows for a pulsation-free feeding of water.

The same cell and the same setup have been used for all spectroscopic experiments described in the following.

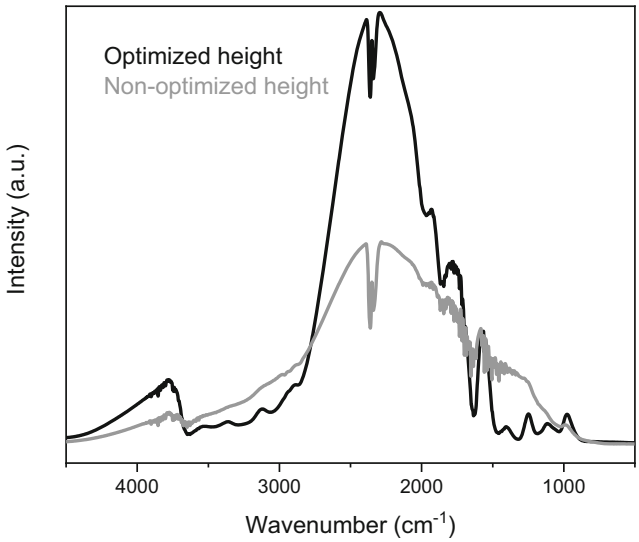


**Fig. 2** Single beam spectra of the sample position (optimized height) and of the window position (non-optimized height) as a function of the cell position in the z-axis

## 2.2 Residence Time Distribution Properties

The residence time distribution (RTD) analysis was performed using a pulse input experiment [22, 34]. NO (2 μL) was introduced in an Ar-only gas feed (100 mL $min^{-1}$) through the cell using a four-way valve. The concentration decay of the tracer was monitored using a Pffeifer Vacuum OmniStar™ mass spectrometer (MS) that was connected downstream of the cell. The experiment was also repeated in a stainless steel gas line bypassing the reactor cell and flowing directly to the MS.

The RTD function $E(t)$ was calculated according to the following formula:

$$E(t) = \frac{C(t)}{\int_0^\infty C(t)dt} \tag{3}$$

where $C(t)$ is the concentration of the tracer leaving the reactor at time $t$. Since NO concentration is directly proportional to the mass-to-charge ratio (m/z) of 30, the latter was used in the calculations. Integrating $E(t)$ over a given time gives the fraction of the gas that has resided in the reactor for that specific period, thus:

$$\int_0^\infty E(t)dt = 1 \quad (4)$$

Experimentally, this relationship is confirmed since the MS signal at m/z = 30 eventually returns to the baseline value after each tracer injection.

An important parameter that can be derived from the RTD analysis is the mean residence time $t_m$:

$$t_m = \int_0^\infty tE(t)dt \quad (5)$$

This is the average time that a molecule spends within the reactor. For transient response studies, a spectroscopic cell with a low $t_m$ is desired.

### 2.3 Catalyst Synthesis and Cell Pre-Treatment

The catalysts used in this study were 2 wt% $V_2O_5/TiO_2$, 2.6 wt% Fe-ZSM-5, and 1.6 wt% Cu-SSZ-13.

$V_2O_5/TiO_2$ was prepared by wet impregnation. A sufficient amount of $NH_4VO_3$ (Fluka, > 99.0%) was dissolved in water at 60 °C, and was mixed for 1 h with $TiO_2$ (DT-51, Cristal) calcined at 550 °C. After removal of water under reduced pressure, the sample was calcined in a muffle furnace at 600 °C for 5 h.

Fe-ZSM-5 was prepared by ion exchange. ZSM-5 (Si/Al = 13; SM-27 P, Süd-Chemie) was mixed with a solution of 0.1 M $FeSO_4 \cdot 7H_2O$ (Sigma-Aldrich, > 99.0%) at room temperature for 6 h. The sample was filtered, washed thrice with distilled water, and dried at 120 °C overnight. Then, it was calcined at 600 °C for 6 h.

Cu-SSZ-13 was prepared by hydrothermal synthesis and ion exchange, as described in detail elsewhere [35]. Briefly, the synthesized SSZ-13 was ion-exchanged with a solution of 0.1 M $CuSO_4 \cdot 5H_2O$ (Sigma-Aldrich, > 98%) at 80 °C for 4 h, filtered, washed thrice with distilled water, and dried at 120 °C overnight. The sample was then calcined at 600 °C for 4 h.

Approximately 50 mg of each catalyst powder (100–150 μm) were loaded in the spectroscopic cell. Prior to each experiment, the sample was dehydrated in 5 vol% $O_2$/Ar (100 mL $min^{-1}$) at 450 °C for 1 h.

### 2.4 ME-Raman Spectroscopy of $V_2O_5/TiO_2$

Raman spectra were collected using a Kaiser RamanRXN-1™ analyzer equipped with a fiber optics probe and a 785-nm laser. Spectra were recorded from 1500 to 100 $cm^{-1}$ at a resolution of 2 $cm^{-1}$ with a laser power of 100 mW and exposure time of 0.5 s. No sample damage was observed under these conditions [33].

The cell was equipped with a 2-mm-thick sapphire window (Crystran) and attached to a Praying Mantis™ accessory. The fiber optics probe was mounted perpendicular to the cell.

ME was performed by pulsing 500 ppm of NO every 30 s in a gas feed of 500 ppm $NH_3$, 2 vol% $H_2O$, 5 vol% $O_2$ balanced in Ar (100 mL $min^{-1}$). Each period consists of 30 consecutive spectra, which are collected every 2 s. At least 20 periods were averaged to generate the phase-resolved spectra.

### 2.5 ME-DR-Vis Spectroscopy of Cu-SSZ-13

Diffuse reflectance visible (DR-Vis) spectra were collected using an Agilent Cary 4000 UV–Vis spectrometer. Spectra were recorded from 350 to 800 nm at a resolution of 1.1 nm and scan rate of 16.7 nm $s^{-1}$. Acquisition in the UV region was not performed because the time resolution would be compromised by changing the light source during the measurement.

The cell was equipped with a 2-mm-thick $CaF_2$ window (Crystran) and attached to a Praying Mantis™ Diffuse Reflection Accessory in the compartment of the UV–Vis spectrometer.

ME was performed by pulsing 1000 ppm NO every 120 s in a gas feed of 1000 ppm $NH_3$, 5 vol% $O_2$ balanced in Ar (100 mL $min^{-1}$). Each period consists of ten consecutive spectra, which are collected every 24 s. At least ten periods were averaged to generate the phase-resolved spectra.

### 2.6 ME-DRIFT Spectroscopy of Fe-ZSM-5

Diffuse reflectance infrared Fourier transform (DRIFT) spectra were collected using a Bruker Vertex70 spectrometer equipped with a HgCdTe detector. Spectra were recorded from 4000 to 1000 $cm^{-1}$ at a resolution of 4 $cm^{-1}$ and scanner velocity of 80 kHz. The sample and background spectra resulted from averaging 10 and 50 scans, respectively.

The cell was equipped with a 2-mm-thick $CaF_2$ window (Crystran) and attached to a Praying Mantis™ accessory in the compartment of the IR spectrometer.

ME was performed by pulsing 1000 ppm NO every 60 s in a gas feed of 1000 ppm $NH_3$, 5 vol% $O_2$ balanced in Ar (100 mL $min^{-1}$). Each period consists of 120 consecutive spectra, which are collected every 1 s. At least 20 periods were averaged to generate the phase-resolved spectra.

### 2.7 Phase-Sensitive Detection

The time-resolved spectra were converted into phase-resolved spectra using the following equation [36]:

$$I\left(\varphi^{PSD}\right) = \frac{2}{T}\int_0^T I(t)\sin\left(k\omega t + \varphi^{PSD}\right)dt \quad (6)$$

where $I(\varphi^{PSD})$ is the intensity or absorbance in the phase-resolved spectra, $T$ is the modulation period, $I(t)$ is the intensity or absorbance in the time-resolved spectra, $k$ is the demodulation index ($k = 1$ in this work), $\omega$ is the stimulation frequency, and $\varphi$ is the phase angle. A Matlab script was used to process the spectra.

## 3 Results and Discussion

### 3.1 RTD Analysis and Mean Residence Time

Residence time distribution (RTD) analysis was performed to check the efficiency of gas exchange inside the reactor. The RTD profile of the NO pulse through the spectroscopic cell was calculated according to Eq. 3, and the results are shown in Table 1 and Fig. 3. At a flow rate of 100 mL $min^{-1}$, the RTD behaviors of the NO pulse through the cell and bypass show very similar shapes. The decay profile of the NO pulse that passed through the cell exhibited tailing, but the effect was offset by the high flow rate.

Decreasing the flow rate broadened the concentration decay curves considerably because of a more pronounced effect of the extra cell volume. The NO concentration reached its maximum value with a considerable time delay—a feature that was not observed at 100 mL $min^{-1}$. At a flow rate of 25 mL $min^{-1}$, the time at which the MS signal decayed to 90% of its initial value ($t_{90}$) was doubled when NO was injected through the cell instead of the bypass.

In all of the decay profiles presented in Fig. 3, the tailing observed as the MS signal returned to the baseline value slowly after the pulse is most probably due to stagnant regions or residual void zones in the cell where the gas exchange might be less efficient. Such profile is characteristic of a non-ideal continuous-stirred tank reactor (CSTR) [34]. Indeed, the commercial cell which served as the basis of the current cell design was reported to be a CSTR according to recently published studies [22, 23]. It is also worth noting that the bypass line also showed a CSTR profile, which is contributed mainly by the MS detection chamber [23].

In modulated excitation experiments, the system will eventually reach a quasi-equilibrium state no matter how large the void volume of the reactor is. However, it is preferred that the concentration of the reactants in the gas phase is changed as much as possible in each half period because this will induce a more prominent change in the corresponding phase-resolved spectra. It is for this reason that the void volume of the spectroscopic cell must be kept to a minimum. For instance, when 1000 ppm NO is pulsed in a feed containing $NH_3$ (i.e., SCR on/off conditions), a reactor with appropriate gas exchange capabilities will allow the NO concentration to drop as close to 0 ppm as possible when the supply is off. On the other hand, a spectroscopic cell with a high void volume might always have various levels of residual NO in the gas phase even though the supply is off. As a result, the SCR reaction is always on and there will be weaker spectral changes to observe after phase-sensitive detection (PSD) treatment.

In the following ME experiments, the total gas flow was fixed at 100 mL $min^{-1}$. The mean residence time ($t_m$) under these conditions was calculated from Eq. 5 to be 22.9 s (Table 1). As a result, we ensured that the half-period of any ME experiment performed with the cell was well above this value (i.e., 30 s for Raman spectroscopy, 60 s for DRIFT spectroscopy, and 120 s for DR-Vis spectroscopy).

**Table 1** Residence time distribution characteristics of the spectroscopic cell

| | Flow rate | | | | | |
|---|---|---|---|---|---|---|
| | 100 mL $min^{-1}$ | | 50 mL $min^{-1}$ | | 25 mL $min^{-1}$ | |
| | Bypass | Cell | Bypass | Cell | Bypass | Cell |
| $t_m$ (s) | 21.6 | 22.9 | 23.8 | 26.2 | 28.4 | 31.2 |
| $t_{90}$ (s) | 2.8 | 3.8 | 4.8 | 6.9 | 7.2 | 13.7 |
| $t_{95}$ (s) | 5.0 | 6.5 | 8.0 | 12.2 | 11.7 | 24.5 |
| $t_{99}$ (s) | 36.6 | 47.3 | 51.0 | 79.6 | 65.3 | 113.4 |

$t_m$ mean residence time, $t_{90}$ time for the MS signal to drop by 90% of the maximum value, $t_{95}$ time for the MS signal to drop by 95% of the maximum value, $t_{99}$ time for the MS signal to drop by 99% of the maximum value

### 3.2 ME-Raman Spectroscopy of $V_2O_5/TiO_2$

Figure 4a, b shows the time-resolved Raman spectra and the corresponding phase-resolved spectra of $V_2O_5/TiO_2$ obtained under repeated NO pulses. The strong bands at 395, 516, and 636 $cm^{-1}$ are characteristic of crystalline $TiO_2$ in the anatase phase, and correspond to $B_{1g}$, $A_{2g} + B_{1g}$, and $E_g$ modes, respectively [37, 38]. The $B_{1g}$ mode has a second overtone at around 800 $cm^{-1}$, which is visible as a weak band in the spectrum. The peak at around 1018 $cm^{-1}$ is readily assigned to the ν(V=O) stretch mode, which is centered at 1031 $cm^{-1}$ under dry, oxidizing conditions [39]. The absence of the bulk $V_2O_5$ peak at 995 $cm^{-1}$ indicates that the $VO_x$ species are well-dispersed in agreement with the submonolayer coverage of the catalyst (2 $VO_x \cdot nm^{-2}$) [40].

Spectral changes were already evident in the time-resolved spectra but were further amplified after PSD. All the three characteristic peaks of $TiO_2$ were strongly perturbed by the periodic NO pulses and thus appeared in the in-phase spectrum shown in Fig. 4b. All other phase-resolved spectra showed the same features but with decreasing intensity. On the other hand, the Raman signal of $VO_x$ was barely discernable even in the phase-resolved spectra. Hence, it appears that $TiO_2$ underwent the most prominent spectral changes during the concentration modulation.

The main role of the support material is to provide a high-surface-area environment that can disperse the active phase. In some instances, however, supports may have a non-innocent role in the catalytic process. In the case of $NH_3$-SCR, $TiO_2$ provides vacant $Ti^{4+}$ sites, where $NH_3$ can adsorb through a Lewis acid-base interaction [17]. Hence, $TiO_2$ serves as a reservoir of

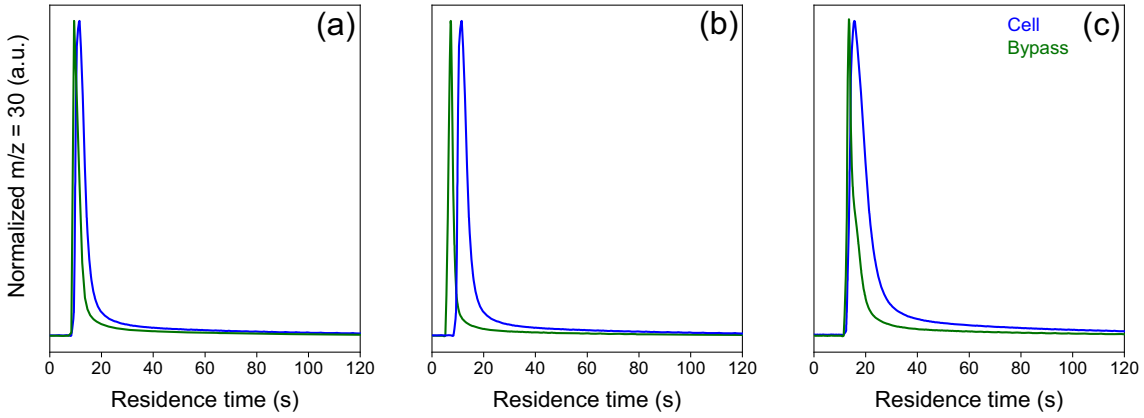


**Fig. 3** Normalized residence time distribution profiles of 2 μL NO pulsed in a gas feed of Ar through the spectroscopic cell and bypass at room temperature and atmospheric pressure in dependence of the total flow: **a** 100 mL $min^{-1}$, **b** 50 mL $min^{-1}$, and **c** 25 mL $min^{-1}$

adsorbed $NH_3$ molecules which can be delivered to the active sites to react if NO is present. In our experiment, $NH_3$ was always present in the gas feed ensuring that the $VO_x$ sites can be supplied with $NH_3$ molecules directly from the gas phase. However, the fact that $TiO_2$ peaks are present in the phase-resolved spectra suggests that the delivery of substrate molecules from $TiO_2$ to $VO_x$ is still at work. Mechanistically, this is intuitively correct since bound $NH_3$ molecules are closer in proximity and easier to access than those that originate from the gas phase. In fact, some studies postulate that $NH_3$ adsorption occurs initially at $TiO_2$ before $VO_x$ sites [41]. This molecular behavior is consistent with the results of our ME experiments.

Most of the $VO_x$ species were coordinated with $NH_3$ and water present in the feed. This is the reason for the position of the ν(V=O) mode in the time-resolved spectra at 1018 $cm^{-1}$ instead of 1031 $cm^{-1}$ [42]. The faint signal of $VO_x$ in the phase-resolved spectra results from the constant presence of $NH_3$ molecules in the gas phase. The reaction between NO and adsorbed $NH_3$ should result ultimately in the production of coordinatively unsaturated $VO_x$ sites. However, this process is so fast that the signal of "free" $VO_x$ is not observed in the phase-resolved spectra under the time scale employed in the experiment. On the other hand, the transfer of $NH_3$ from neighboring $TiO_2$ to the active sites is probably slower, which explains why the characteristic peaks of $TiO_2$ are present in the phase-resolved spectra. In a complementary experiment where $NH_3$ is pulsed in a gas feed containing a constant concentration of NO, the signal of coordinatively unsaturated

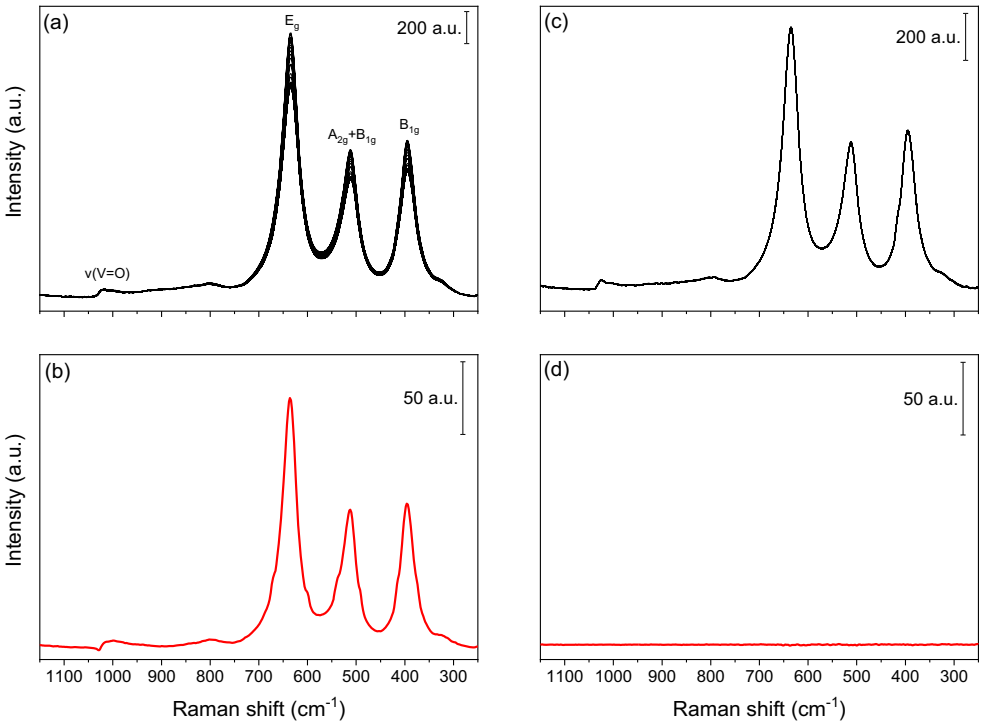


**Fig. 4** **a** Time-resolved Raman spectra and **b** the corresponding in-phase spectrum of $V_2O_5/TiO_2$ at 250 °C during 30-s pulses of 500 ppm NO in a gas feed of 500 ppm $NH_3$, 2 vol% $H_2O$ and 5 vol% $O_2$ balanced in Ar. **c** Time-resolved Raman spectra and **d** a selected phase-resolved spectrum of 2 wt% $V_2O_5/TiO_2$ at 250 °C during 30-s pulses of Ar in a gas feed of 2 vol% $H_2O$ and 5 vol% $O_2$ balanced in Ar

$VO_x$ species was present in the phase-resolved spectra [33]. This proves that vacant $VO_x$ species are indeed formed during the reaction cycle and can be observed when a strongly adsorbing species such as $NH_3$ is not constantly present.

To confirm that the observed effect is in fact due to the SCR reaction, a control experiment was performed in the absence of SCR activity (Fig. 4c, d). This was achieved by pulsing Ar in a gas feed containing 2 vol% $H_2O$ and 5 vol% $O_2$ balanced in Ar. Although the time-resolved spectra showed all of the expected signals of $VO_x$ and $TiO_2$, the phase-resolved spectra did not present any signal. This means that neither $VO_x$ nor $TiO_2$ was perturbed by the inert gas pulsing.

### 3.3 ME-DR-Vis Spectroscopy of Cu-SSZ-13

The active Cu site in the catalyst changes reversibly between two oxidation states (i.e., + 2 and + 1) during the course of the SCR reaction [19]. Cu(II) exhibits a *d-d* transition band in the region of 500–1100 nm and when it is supported on a zeolite, it has an additional band at 220–380 nm due to ligand-to-metal charge transfer (LMCT) [43]. In contrast, Cu(I) does not possess a *d-d* transition band because of its fully filled 3d shell. Hence, the reversible Cu(II)↔Cu(I) redox changes in Cu-SSZ-13 can be monitored by following the appearance/disappearance of the characteristic bands of Cu(II).

The time-resolved and phase-resolved DR-Vis spectra as a result of repeated NO pulsing are presented in Fig. 5a, b. The time-resolved spectra show very shallow bands in the region of 350–800 nm, but no obvious changes were observed. The difference spectra between Cu-SSZ-13 under $NH_3$ and $NH_3$/NO gas feeds could potentially reveal the characteristic Cu(II) bands, but the signal-to-noise-ratio is low (Fig. S-6). Hence, the application of PSD is justified to accentuate the spectral changes. The in-phase spectrum in Fig. 4b is very similar to the difference spectrum and exhibits a broad band above 500 nm that may be associated with the *d-d* transition band of Cu(II). The band extending below 430 nm originates from LMCT (in particular, $O^{2-} \rightarrow Cu^{2+}$) and is not complete in the UV region because the acquisition was stopped at 350 nm to meet the required time resolution. These two bands vary in-phase (i.e., they increase and decrease simultaneously) because they both originate from the same chemical entity. All other phase-resolved spectra show only intensity variations of these two features.

Without SCR activity (i.e., in the absence of NO), most of the Cu species are in the + 2 oxidation state, according to the generally accepted reaction mechanism [19]. The presence of both $NH_3$ and NO is needed to drive the reduction of Cu(II) to Cu(I), which is coordinated to both reactants and from which the nitrosamide intermediate forms. Although $NH_3$ alone can reduce Cu(II) in some Cu-based catalysts [44], temperatures higher than 250 °C are required. It is therefore the NO pulsing that induces the redox process in the experiment presented in Fig. 5.

Also in this case, a control experiment was performed in the absence of SCR activity by repeated Ar pulses (Fig. 5c, d). No signal was observed in the phase-resolved spectrum, which confirms that the bands observed in Fig. 5b clearly originate from the redox process of the Cu sites during SCR activity.

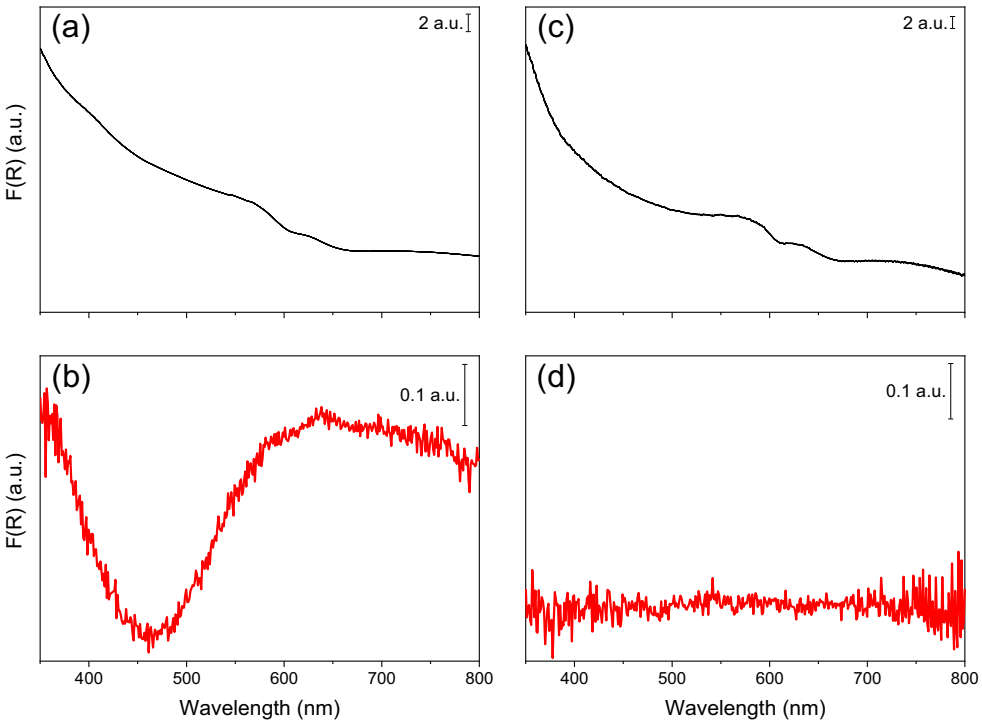


**Fig. 5** **a** Time-resolved DR-Vis spectra and **b** the corresponding in-phase spectrum of 1.6 wt% Cu-SSZ-13 at 250 °C during 120-s pulses of 1000 ppm NO in a gas feed of 1000 ppm $NH_3$, 2 vol% $H_2O$, and 5 vol% $O_2$ balanced in Ar. **c** Time-resolved DR-Vis spectra and **d** a selected phase-resolved spectrum of 1.6 wt% Cu-SSZ-13 at 250 °C during 120-s pulses of Ar in a gas feed of 2 vol% $H_2O$ and 5 vol% $O_2$ balanced in Ar

### 3.4 ME-DRIFT Spectroscopy of Fe-ZSM-5

Figure 6a, b shows the time-resolved and phase-resolved DRIFT spectra as a result of NO pulses in $NH_3$ while Fig. 6c, d shows the equivalent set of spectra as a result of Ar pulses in $NH_3$. The time-resolved spectra of both experiments are practically identical—they are both dominated by the signal contribution from adsorbed water and $NH_3$. This is equally evident in the stretching region in 3500–2500 $cm^{-1}$ and the bending region (1750–1250 $cm^{-1}$) as well. As a result, it is hard to rationalize the presence of other adsorbates and intermediates on the catalyst surface. NO, for instance, is also expected to adsorb on the catalyst under these experimental conditions [45]. Some studies also hinted at the formation of NO-derived species such as nitrates, especially at lower temperatures [46]. However, the weak signal of adsorbed NO and its potential derivatives compared to water and $NH_3$ precludes their unequivocal identification in the time-resolved spectra.

On the contrary, the phase-resolved spectra uncovered substantial differences between the two experiments. When NO was pulsed, several signals were perturbed and appeared in the phase-resolved spectra. For example, hydroxyl (–OH; 3650 $cm^{-1}$), residual sulfate (–$SO_4$; 1365 $cm^{-1}$) from the ion-exchange procedure, adsorbed $NH_3$ (3350–3150 $cm^{-1}$), and nitrosyl ($NO^+$; 2139 $cm^{-1}$) species were perturbed. The –OH and –$SO_4$ groups varied out-of-phase (i.e., exhibited opposite signal variation) with $NH_3$ and $NO^+$ because they are being titrated upon adsorption. When only Ar was pulsed (Fig. 6c, d), the apparent signals in the selected phase-resolved spectrum are negligible compared with the experiment under SCR conditions. Furthermore, the presence of the phase-resolved signal of $NH_3$ in Fig. 6b suggests that it is being consumed during the NO pulsing, proving the occurrence of the SCR reaction.

The peaks in the region of 3350-3150 $cm^{-1}$ in Fig.6a correspond to $NH_3$ adsorbed on Brønsted–Lowry sites and Lewis acid sites [47, 48]. The former are present in the zeolite framework due to the charge imbalance of Al–O–Si bonds while the latter can be attributed predominantly to the coordinatively unsaturated Fe sites. In the time-resolved spectra, the two adsorption sites are not well-resolved because adsorbed water also provides a broad overlapping signal in this region of the spectrum. However, the characteristic N-H bending peaks were

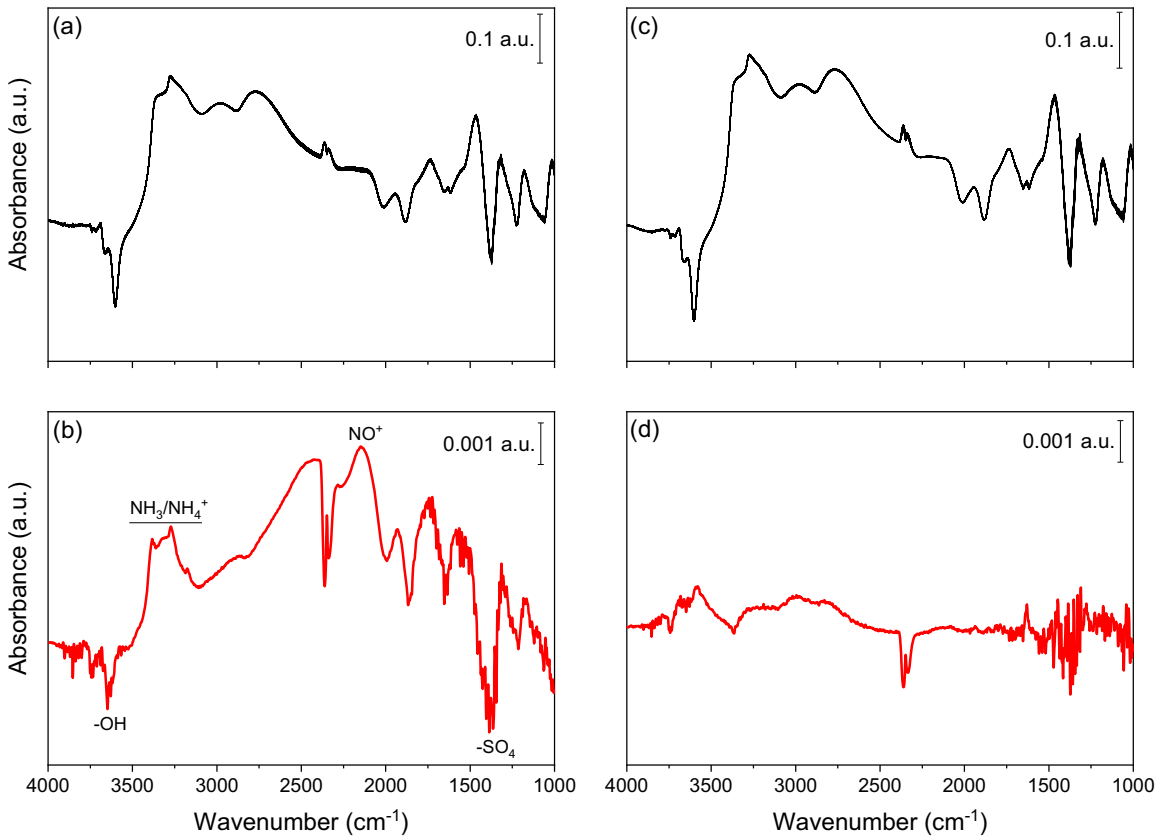


**Fig. 6** **a** Time-resolved DRIFT spectra and **b** the corresponding in-phase spectrum of 2.6 wt% Fe-ZSM-5 at 250 °C during 60-s pulses of NO in a gas feed of 1000 ppm $NH_3$, 2 vol% $H_2O$ and 5 vol% $O_2$ balanced in Ar. **c** Time-resolved DRIFT spectra and **d** a selected phase-resolved spectrum of 1 wt% Fe-ZSM-5 at 250 °C during 60-s pulses of Ar in a gas feed of 1000 ppm $NH_3$, 2 vol% $H_2O$ and 5 vol% $O_2$ balanced in Ar. The peaks at 2360 and 2330 $cm^{-1}$ originate from fluctuations in $CO_2$ concentration in the environment of the sample compartment and not from any adsorbed species

revealed after PSD treatment. Hence, it appears from the phase-resolved spectra that both the active Fe sites and the support (Brønsted–Lowry sites) coordinate with $NH_3$ molecules. Steady-state catalytic tests have revealed that the metal-free ZSM-5 support did not exhibit any appreciable SCR activity at 250 °C (and even up to 450 °C). This means that it is the Fe active site that is solely responsible for the SCR activity, which rationalizes the perturbation of Lewis-bound $NH_3$ due to NO pulses. However, $NH_3$ bound to Brønsted–Lowry sites were also perturbed by NO, indicating that during the pulse duration, they might be transferred to Fe sites to react as well.

## 4 Conclusions

We have presented a reactor cell with a low void volume that can be used for ME spectroscopic studies such as (1) Raman spectroscopy of $V_2O_5/TiO_2$; (2) DR-Vis spectroscopy of Cu-SSZ-13; and (3) DRIFT spectroscopy of Fe-ZSM-5. Due to the low void volume of the cell, the gases were exchanged very efficiently in every pulse sequence, which induced large spectroscopic response after PSD treatment. The results presented here are obviously not sufficient to draw full mechanistic conclusions; rather, they are case studies targeted to prove the suitability of the cell for transient response and ME experimentation. The demonstrated versatility of the cell with regard to various spectroscopic techniques paves the way for implementing time-resolved structural studies which are truly complementary with one another.

**Acknowledgments** The authors acknowledge the financial support from the Swiss National Science Foundation (SNF, Project #200021_172669/1). The authors are grateful to H. Altorfer for the cell drawings, M. Hottinger for the cell fabrication, and P. Hottiger for the electrical connections. This project was carried out in the framework of the Swiss Competence Center for Energy Research (SCCER) BIOSWEET program.

### Compliance with Ethical Standards

**Conflict of Interest** The authors declare that they have no conflict of interest.

## References

1. Kummer, J.T.: Catalysts for automobile emission control. Prog. Energy Combust. Sci. **6**(2), 177–199 (1980)
2. Cooper, B.J.: Challenges in emission control catalysis for the next decade. Platin. Met. Rev. **38**(1), 2–10 (1994)
3. Jobson, E.: Future challenges in automotive emission control. Top. Catal. **28**(1), 191–199 (2004)
4. Johnson, T.: Vehicular emissions in review. SAE Int. J. Engines. **9**(2), 1258–1275 (2016)
5. Tayyeb Javed, M., Irfan, N., Gibbs, B.M.: Control of combustion-generated nitrogen oxides by selective non-catalytic reduction. J. Environ. Manag. **83**(3), 251–289 (2007)
6. Cheng, X., Bi, X.T.: A review of recent advances in selective catalytic $NO_x$ reduction reactor technologies. Particuology. **16**, 1–18 (2014)
7. Roy, S., Baiker, A.: $NO_x$ storage–reduction catalysis: From mechanism and materials properties to storage–reduction performance. Chem. Rev. **109**(9), 4054–4091 (2009)
8. Kröcher, O.: Aspects of catalyst development for mobile urea-SCR systems—From vanadia-titania catalysts to metal-exchanged zeolites. In: Granger, P., Pârvulescu, V.I. (eds.) Studies in Surface Science and Catalysis, vol. 171, pp. 261–289. Elsevier (2007)
9. Nova, I., Tronconi, E.: Urea-SCR technology for de$NO_x$ after treatment of diesel exhausts. Springer, New York (2014)
10. Ciardelli, C., Nova, I., Tronconi, E., Chatterjee, D., Bandl-Konrad, B.: A "Nitrate Route" for the low temperature "Fast SCR" reaction over a $V_2O_5$–$WO_3/TiO_2$ commercial catalyst. Chem. Commun. **23**, 2718–2719 (2004)
11. Amiridis, M., Wachs, I., Deo, G., Jehng, J.-M., Soung Kim, D.: Reactivity of $V_2O_5$ catalysts for the selective catalytic reduction of NO by $NH_3$: influence of Vanadia loading, $H_2O$, and $SO_2$. J. Catal. **161**(1), 247–253 (1996)
12. Kharas, K.C.C., Robota, H.J., Liu, D.J.: Deactivation in Cu-ZSM-5 lean-burn catalysts. Appl. Catal. B Environ. **2**(2), 225–237 (1993)
13. Kwak, J.H., Tonkyn, R.G., Kim, D.H., Szanyi, J., Peden, C.H.F.: Excellent activity and selectivity of Cu-SSZ-13 in the selective catalytic reduction of $NO_x$ with $NH_3$. J. Catal. **275**(2), 187–190 (2010)
14. Wang, J., Zhao, H., Haller, G., Li, Y.: Recent advances in the selective catalytic reduction of $NO_x$ with $NH_3$ on Cu-Chabazite catalysts. Appl. Catal. B Environ. **202**, 346–354 (2017)
15. Kamasamudram, K., Currier, N., Szailer, T., Yezerets, A.: Why Cu- and Fe-zeolite SCR catalysts behave differently at low temperatures. SAE Int. J. Fuels Lubr. **3**(1), 664–672 (2010)
16. Colombo, M., Nova, I., Tronconi, E.: A comparative study of the $NH_3$-SCR reactions over a Cu-zeolite and a Fe-zeolite catalyst. Catal. Today. **151**(3), 223–230 (2010)
17. Ramis, G., Busca, G., Bregani, F., Forzatti, P.: Fourier transform-infrared study of the adsorption and coadsorption of nitric oxide, nitrogen dioxide and ammonia on vanadia-titania and mechanism of selective catalytic reduction. Appl. Catal. **64**, 259–278 (1990)
18. Topsøe, N.-Y.: Mechanism of the selective catalytic reduction of nitric oxide by ammonia elucidated by in situ on-line Fourier transform infrared spectroscopy. Science. **265**(5176), 1217–1219 (1994)
19. Janssens, T.V.W., Falsig, H., Lundegaard, L.F., Vennestrøm, P.N.R., Rasmussen, S.B., Moses, P.G., Giordanino, F., Borfecchia, E., Lomachenko, K.A., Lamberti, C., Bordiga, S., Godiksen, A., Mossin, S., Beato, P.: A consistent reaction scheme for the selective catalytic reduction of nitrogen oxides with ammonia. ACS Catal. **5**(5), 2832–2845 (2015)
20. Müller, P., Hermans, I.: Applications of modulation excitation spectroscopy in heterogeneous catalysis. Ind. Eng. Chem. Res. **56**(5), 1123–1136 (2017)
21. Meunier, F.C.: The design and testing of kinetically-appropriate operando spectroscopic cells for investigating heterogeneous catalytic reactions. Chem. Soc. Rev. **39**(12), 4602–4614 (2010)
22. Srinivasan, P.D., Nitz, S.R., Stephens, K.J., Atchison, E., Bravo-Suarez, J.J.: Modified Harrick reaction cell for in situ/operando fiber optics diffuse reflectance UV–visible spectroscopic characterization of catalysts. Appl. Catal. A Gen. **561**, 7–18 (2018)
23. Patil, B.S., Srinivasan, P.D., Atchison, E., Zhu, H., Bravo-Suárez, J.J.: Design, modelling, and application of a low void-volume in situ diffuse reflectance spectroscopic reaction cell for transient catalytic studies. React. Chem. Eng. **4**(4), 667–678 (2019)

24. Chiarello, G.L., Nachtegaal, M., Marchionni, V., Quaroni, L., Ferri, D.: Adding diffuse reflectance infrared Fourier transform spectroscopy capability to extended x-ray-absorption fine structure in a new cell to study solid catalysts in combination with a modulation approach. Rev. Sci. Instrum. **85**(7), 074102 (2014)
25. Schubert, M.M., Häring, T.P., Bräth, G., Gasteiger, H.A., Behm, R.J.: New DRIFTS cell design for the simultaneous acquisition of IR spectra and kinetic data using on-line product analysis. Appl. Spectrosc. **55**(11), 1537–1543 (2001)
26. Bansode, A., Guilera, G., Cuartero, V., Simonelli, L., Avila, M., Urakawa, A.: Performance and characteristics of a high pressure, high temperature capillary cell with facile construction for operando x-ray absorption spectroscopy. Rev. Sci. Instrum. **85**(8), 084105 (2014)
27. Dal Santo, V., Dossi, C., Fusi, A., Psaro, R., Mondelli, C., Recchia, S.: Fast transient infrared studies in material science: Development of a novel low dead-volume, high temperature DRIFTS cell. Talanta. **66**(3), 674–682 (2005)
28. Wachs, I.E.: Raman and IR studies of surface metal oxide species on oxide supports: Supported metal oxide catalysts. Catal. Today. **27**(3), 437–455 (1996)
29. Weckhuysen, B.M., Schoonheydt, R.A.: Recent progress in diffuse reflectance spectroscopy of supported metal oxide catalysts. Catal. Today. **49**(4), 441–451 (1999)
30. Lamberti, C., Zecchina, A., Groppo, E., Bordiga, S.: Probing the surfaces of heterogeneous catalysts by in situ IR spectroscopy. Chem. Soc. Rev. **39**(12), 4951–5001 (2010)
31. Marberger, A., Ferri, D., Elsener, M., Kröcher, O.: The significance of Lewis acid sites for the selective catalytic reduction of nitric oxide on vanadium-based catalysts. Angew. Chem. Int. Ed. **55**(39), 11989–11994 (2016)
32. Sridhar, M., Ferri, D., van Bokhoven, J.A., Kröcher, O.: Water-assisted oxygen activation during gold-catalyzed formic acid decomposition under SCR-relevant conditions. J. Catal. **349**, 197–207 (2017)
33. Nuguid, R.J.G., Ferri, D., Marberger, A., Nachtegaal, M., Kröcher, O.: Modulated excitation Raman spectroscopy of $V_2O_5/TiO_2$: Mechanistic insights into the selective catalytic reduction of NO with $NH_3$. ACS Catal. **9**(8), 6814–6820 (2019)
34. Fogler, H.S.: Distribution of residence times for chemical reactors. In: Elements of Chemical Reaction Engineering, pp. 867–944. Prentice Hall, Upper Saddle River (2005)
35. Marberger, A., Petrov, A.W., Steiger, P., Elsener, M., Kröcher, O., Nachtegaal, M., Ferri, D.: Time-resolved copper speciation during selective catalytic reduction of NO on Cu-SSZ-13. Nat. Catal. **1**(3), 221–227 (2018)
36. Baurecht, D., Fringeli, U.P.: Quantitative modulated excitation Fourier transform infrared spectroscopy. Rev. Sci. Instrum. **72**(10), 3782–3792 (2001)
37. Ohsaka, T., Izumi, F., Fujiki, Y.: Raman spectrum of anatase, $TiO_2$. J. Raman Spectrosc. **7**(6), 321–324 (1978)
38. Frank, O., Zukalova, M., Laskova, B., Kürti, J., Koltai, J., Kavan, L.: Raman spectra of titanium dioxide (anatase, rutile) with identified oxygen isotopes (16, 17, 18). Phys. Chem. Chem. Phys. **14**(42), 14567–14572 (2012)
39. Went, G.T., Oyama, S.T., Bell, A.T.: Laser Raman spectroscopy of supported vanadium oxide catalysts. J. Phys. Chem. **94**(10), 4240–4246 (1990)
40. Wachs, I.E., Weckhuysen, B.M.: Structure and reactivity of surface vanadium oxide species on oxide supports. Appl. Catal. A Gen. **157**(1), 67–90 (1997)
41. Tronconi, E., Nova, I., Ciardelli, C., Chatterjee, D., Weibel, M.: Redox features in the catalytic mechanism of the "standard" and "fast" $NH_3$-SCR of $NO_x$ over a V-based catalyst investigated by dynamic methods. J. Catal. **245**(1), 1–10 (2007)
42. Giakoumelou, I., Fountzoula, C., Kordulis, C., Boghosian, S.: Molecular structure and catalytic activity of $V_2O_5/TiO_2$ catalysts for the SCR of NO by $NH_3$: in situ Raman spectra in the presence of $O_2$, $NH_3$, NO, $H_2$, $H_2O$, and $SO_2$. J. Catal. **239**(1), 1–12 (2006)
43. Negri, C., Signorile, M., Porcaro, N.G., Borfecchia, E., Berlier, G., Janssens, T.V.W., Bordiga, S.: Dynamic $Cu^{II}/Cu^{I}$ speciation in Cu-CHA catalysts by in situ diffuse reflectance UV–vis-NIR spectroscopy. Appl. Catal. A Gen. **578**, 1–9 (2019)
44. Nanba, T., Chino, T., Masukawa, S., Uchisawa, J., Obuchi, A.: Total oxidation of toluene over $Cu/TiO_2/SiO_2$. Bull. Chem. Soc. Jpn. **86**(4), 534–539 (2013)
45. Long, R.Q., Yang, R.T.: Characterization of Fe-ZSM-5 catalyst for selective catalytic reduction of nitric oxide by ammonia. J. Catal. **194**(1), 80–90 (2000)
46. Schwidder, M., Heikens, S., De Toni, A., Geisler, S., Berndt, M., Brückner, A., Grünert, W.: The role of $NO_2$ in the selective catalytic reduction of nitrogen oxides over Fe-ZSM-5 catalysts: Active sites for the conversion of NO and of $NO/NO_2$ mixtures. J. Catal. **259**(1), 96–103 (2008)
47. Devadas, M., Kröcher, O., Elsener, M., Wokaun, A., Mitrikas, G., Söger, N., Pfeifer, M., Demel, Y., Mussmann, L.: Characterization and catalytic investigation of Fe-ZSM5 for urea-SCR. Catal. Today **119**(1), 137–144 (2007)
48. Elzey, S., Mubayi, A., Larsen, S.C., Grassian, V.H.: FTIR study of the selective catalytic reduction of $NO_2$ with ammonia on nanocrystalline NaY and CuY. J. Mol. Catal. A: Chem. **285**(1), 48–57 (2008)


**Publisher's Note** Springer Nature remains neutral with regard to jurisdictional claims in published maps and institutional affiliations.